Experimental and Numerical Description of Mineral Precipitation Dynamics on Heterogeneous Substrate Surfaces

Mohammad Nooraiepour[1, *], Mohammad Masoudi[1] and Helge Hellevang[1]

[1] Department of Geosciences, University of Oslo, P.O. Box 1047 Blindern, 0316 Oslo, Norway
* Correspondence: mohammad.nooraiepour@geo.uio.no

Experimental and Numerical Description of Mineral Precipitation Dynamics on Heterogeneous Substrate Surfaces

Mohammad Nooraiepour[1*], Mohammad Masoudi[1*] and Helge Hellevang[1]

[1] Department of Geosciences, University of Oslo, P.O. Box 1047 Blindern, 0316 Oslo, Norway

mohammad.nooraiepour@geo.uio.no

Keywords: Nucleation; Precipitation; Crystal Growth; Crystallite Formation; Reactive Transport; Geometry Alteration.

ABSTRACT

Mineral precipitation reactions are critical in reactive transport studies of porous media due to their significant impacts on flow and transport properties. Understanding the nucleation process, a probabilistic phenomenon that determines the location and distribution of solid formation in space and time domains, is essential for accurately comprehending the effect of mineral precipitation on porous media surfaces. To this end, this paper presents microfluidic laboratory experiments and reactive transport modeling of mineral precipitation dynamics under different physicochemical conditions and substrate surface properties. Our results demonstrate the importance of the spatial and temporal location and distribution of nucleation and growth events when the interplay among several determining parameters is inevitable. We show mineral precipitation on primary and secondary substrate surfaces under different supersaturations and temperatures. Our high-resolution EDS-SEM surface maps identify the favorable sites and competing locations for attracting solute concentration and continued growth, providing valuable insights into the mineral precipitation mechanism.

1. INTRODUCTION

Interface-coupled precipitation and dissolution geochemical reactions are crucial in studying the coupled thermo-hydro-mechanical-chemical (THMC) phenomena and processes in subsurface environments. Understanding these reactions is vital for addressing pressing energy, environmental, and societal challenges, including carbon dioxide (CO_2) storage and geothermal energy. Mineral nucleation and growth exemplify interface-coupled dissolution and precipitation reactions that alter the geometry of porous media. When precipitation reactions are abundant, crystal accumulations can substantially reduce porosity, which alters the connectivity of the pore space and affects properties such as tortuosity and permeability. Additionally, precipitation changes the available surface area for growth, leading to modifications in the system's reactivity, reaction progress, and rates. It is critical to understand and predict the parameters and mechanisms governing mineral precipitation to evaluate geochemical coupled THMC fluid-rock interactions and their effects on geoenergy and geoenvironmental systems

Understanding the consequences of mineral precipitation (i.e., nucleation and crystal growth) within the porous medium and the fate of fluid flow and solute transport requires spatial and temporal knowledge of the location and amount of solid precipitation. The reactive transport models (RTMs) only then can provide precise and realistic predictions on the intricate interplay between transport mechanisms and reaction kinetics and, therefore, advection-diffusion-reaction (ADR). However, accurately representing the dynamics and dimensionality of mineral precipitation in porous media is still challenging. The complexity of RTMs arises from their dependence on multiple parameters, including fluid flow, fluid chemistry, and the mineral substrate, which can vary significantly over different time- and length-scales. Prediction of these complex perturbations requires RTMs that are often far from trivial because of the simultaneous dynamic interplay of the several parameters in action.

We conducted laboratory microfluidic experiments on actual rocks and utilized reactive Lattice Boltzmann Method (LBM) simulations to investigate the spatial distribution of mineral precipitation events under different physiochemical conditions. Here, we build on our previous reports on probabilistic nucleation and growth (Hellevang et al., 2019; Nooraiepour et al., 2022). Our results highlight the significance of the precise spatial and temporal location and distribution of nucleation and crystal growth events in the presence of several determining parameters. Furthermore, we demonstrate that probabilistic nucleation leads to stochastic distributions in the quantity and location of crystals in both temporal and spatial domains.

2. MATERIALS AND METHODS

2.1 Batch-type microfluidic experiments

A natural heterogeneous (multi-mineral) sandstone was selected as a geomaterial substrate (disk shape specimens of 1.5 cm height and 2.5 cm diameter). For the calcium carbonate synthesis, we prepared stock solutions from respective crystalline solids (ACS reagent, ≥ 99.8%) of calcium chloride ($CaCl_2$) and sodium bicarbonate ($NaHCO_3$) by adding the well-defined weight of salts to the deionized-water (Milli-Q water). We used the PHREEQC package for aqueous geochemical calculations to compute solute supersaturation. The supersaturation (Ω) is defined as the saturation ratio given by the ion activity product divided by the equilibrium constant. Nine experiments were conducted at three supersaturations (Ω = 15, 50, and 130x) and three temperatures (T = 20, 40, and 60°C). For each Ω, experiments at three different temperatures were performed. The elapsed times (t) were 6, 48, and 96 hours. Therefore, a total of 27 experiments (3×3×3 sets of Ω-T-t) were carried out. Further details of the laboratory procedure (Nooraiepour et al., 2021b, 2022) and setup (Moghadam et al., 2019; Fazeli et al., 2021) were given in our previous publications. Scanning electron microscopy (SEM) via backscattered (BSE) and secondary electrons (SE) imaging was used to study the surface structure and mineral growth. The energy-dispersive x-ray spectroscopy (EDS) was used for chemical analyses and element mapping. Three random locations were selected and analyzed for SEM-EDS surface mapping for each substrate. A mosaic map of nine SEM-EDS images

covering an approximately 10.5 mm^2 area was acquired with a spatial resolution of 1 µm. A variable pressure Hitachi SU5000 FE-SEM (Schottky FEG) equipped with a Dual Bruker XFlash system was used to perform the SEM imaging and EDS spectroscopy.

2.2 LBM reactive numerical simulation

For the numerical simulation of surface mineral growth, we used the Lattice Boltzmann (LB) model to solve the advection-diffusion-reaction (ADR) equations for tracking the concentration of different species. We developed a reactive transport model based on our recently proposed probabilistic nucleation and crystal growth theory. In the proposed model and the LBM implementation, both location and time of nucleation are probabilistic (spatiotemporal stochastic dynamics), which may significantly impact the evolution of transport properties across time and length scales. Our previous works include details of probabilistic nucleation and how to implement it into pore-scale reactive transport models (Nooraiepour et al., 2021a, 2022; Masoudi et al., 2021). The D2Q9 lattice scheme was used in a 400×400 µm simulation domain representing a homogeneous nonreactive substrate and a dual substrate system to model the surface nucleation and growth. All boundaries are subject to periodic boundary conditions. The domain is initially oversaturated with mineral A. An infinite source of a solution on top of the substrate was imposed. The first step in the LBM simulations is probabilistic nucleation, which is the necessary condition for growth or for the reaction to start {A(aq) ⇄ A(s)}. As we previously showed, the nucleation and growth of the secondary phase on the initial substrate will create a new substrate in which nucleation will be more likely to occur. This is implemented into the model using weighted arithmetic averaging based on the surface area. Three simulation scenarios for the dual substrate system are designed to evaluate the effect of relative interfacial free energy on the mineral distribution. The proportionality ratio of subdomains is as follows σ_2/σ_1 = [0.5, 1, 1.6]. The interfacial free energy of the bottom-left and top-right parts of the domain is different from the rest.

3. Results and Discussion

3.1 Probabilistic dynamics of mineral precipitation

Figure 1 presents the EDS-SEM surface maps of calcium carbonate precipitations (color-coded in green) on heterogeneous sandstone substrate, where mineral precipitation is compared for two supersaturations Ω = 15x (top) and 130x (bottom) at two temporal stages. In the low supersaturation case, precipitation started on the intergranular carbonate cement patches as a favorable nucleation and crystal growth site (Fig. 1a). With the increase in elapsed time, then a number of precipitation sites with limited growth were developed (Fig. 1b). For the high supersaturation, however, fast and extensive nucleation (via identification of crystallite formations) and growth is observed in Figure 1c. The number of crystals and their surface coverage then increases as the precipitation reaction progresses. Therefore, two trends are evident in Figure 1. An increase in Ω and extended t contributed to an increase in the number and the total coverage area of crystals. The patch sizes (connected precipitates) also increase at higher Ω-t conditions. The impact of extended elapsed time from the onset of the experiment is pronounced for higher supersaturations, owing to the continued and available solute concentration in the substrate's proximity within the aqueous phase. Comparison between the different supersaturations suggests that at lower Ω values, a more selective pattern for the location of crystal nucleation and growth can be identified. In high supersaturations (Ω = 130, Figs. 1c-d), an overall closely packed pattern is observable where crystals tend to cover the surface of the substrate more uniformly.

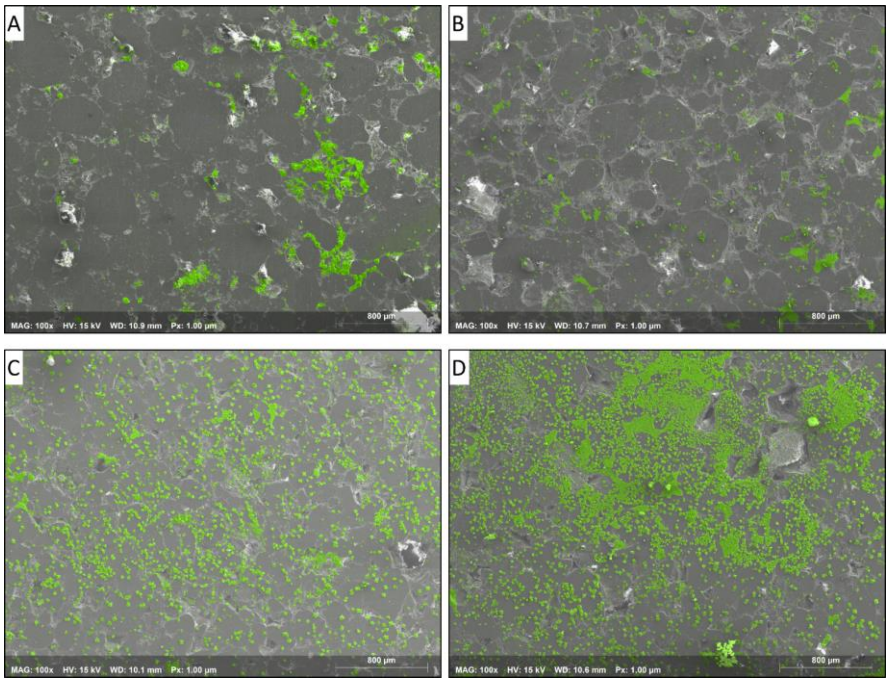

Figure 1: Surface mineral precipitation maps at (top) 15x and (bottom) 130 supersaturations (Ω) at two stages of elapsed times from the onset of the experiment (t) for the laboratory tests conducted at temperature T = 60 °C. The mosaic maps demonstrate the superimposed EDS on top of the BSE SEM to identify calcium carbonate crystals (color-coded in green). Each mosaic map covers a 10.5 mm^2 area with a spatial resolution of 1 µm. Magnification: 100x.

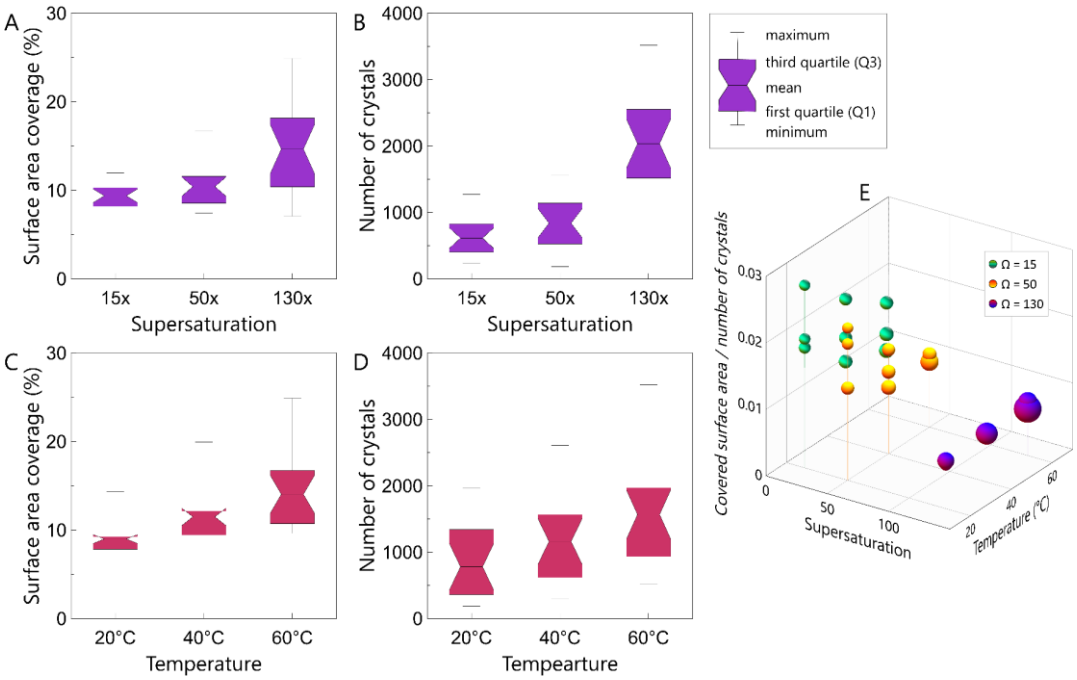

Figure 2: Box plots of surface area coverage (%) and the number of crystals as a function of (top, a-b) supersaturation and (bottom, c-d) temperature, obtained by digital image analysis of precipitation maps. It shows skewness, quartiles (25% and 75%), mean, and minimum and maximum whiskers. (e) Ratio of average covered surface area divided by crystals number versus temperature and supersaturation. The size of the balls illustrates the average covered surface area.

Image processing results of 27 experiments (3×3×3 sets of Ω-T-t) are presented in Figure 2, where surface area coverage (%) and the number of crystals are plotted as a function of supersaturation and temperature in boxplots. The data distribution, skewness, quartiles (25% and 75% percentiles), and mean values are shown. The whiskers (lines extending from the box plots) represent the minimum and maximum measured values. Figure 2 demonstrates the significant effects of solute supersaturation and temperature on mineral precipitation. The distance between minimum and maximum (variability domain) is increased with the increase in Ω and T. Comparison between the effect of Ω and T shows that the expected variability and scatter at a given T is more significant than at a given Ω (Fig. 2). It highlights the effect of temperature on the randomness of crystal formation and deposition patterns and more considerable variations that one may expect when temperature changes compared to supersaturation.

The crystal coverage area and count increased remarkably for higher Ω values, particularly for Ω = 130. The increase in the coverage area and crystal counts over time for a given Ω are subtle for T = 20°C compared to elevated Ts. The area-to-count ratio shows a decline with the increase in temperature and supersaturation. The scatter in data points at a given condition (fixed T-Ω) also decreased at higher T- Ω values. In lower supersaturations, the probability of nucleation is lower. As a result, fewer numbers of stable nuclei form at an early time. These stable nuclei consume the available solute in the solution to grow, decreasing the probability of new nucleation events. Low supersaturations bring about more connected and more extensive solid accumulations. However, when the saturation ratio is high (Ω = 130), the driving force for growth and nucleation is significant, and scattered patterns might also form. In other words, the low Ω case is associated with the limited solute concentration, limiting the number of new nucleations, therefore less supporting the continued growth of previously precipitated solids at early times. At higher supersaturations (Ω = 130), enough solute is present in the solution to support continued nucleation and growth of crystals.

In Figure 2e, the ratio of the average covered surface area (%) divided by the number of precipitated crystals is given in the z-axis as a function of temperature and supersaturation. The size of the balls illustrates the average covered surface area. The area-to-count ratio shows a decline with the increase in temperature and supersaturation. The impact of supersaturation is particularly pronounced. The lower area-to-count ratio at higher supersaturations can be associated with higher nucleation events and growth sites at higher T-Ω, which did not coalesce and form interconnected pockets with comparable areal coverage. In other words, at lower Ω, a comparatively limited number of nuclei manage to crystallize and continue to form growth sites. These growth sites will then be able to attract available solute concentrations and produce more extensive pockets/patches of mineral accumulations. Therefore, fewer crystals and more extensive individual accumulations result in a higher area-to-count ratio at lower Ω (or T-Ω) conditions. Additionally, the scatter in data points at a given condition (fixed T-Ω) also decreased at higher T-Ω values (Fig. 2). The more scatter in lower T-Ω pairs and the limited growth sites suggest that system randomness might be higher.

3.2 Mineral precipitation on primary and secondary substrates

This section provides visual evidence of high-resolution scanning electron microscopy of mineral precipitation on primary and secondary substrates. In Figure 3, crystallite formation and mineral growth on the foreign substrate (as a result of heterogeneous nucleation) and previously precipitated crystals are presented. Additionally, precipitation of primitive forms on crystals is shown down to sub-micron resolution. For reactive transport modeling (RTM) of mineral nucleation and growth, one may hypothesize that the ratio between the reaction rate and nucleation rate solely controls the growth pattern and can be used as a proxy for predicting geometry evolution in the porous medium across scales. However, present results refute the hypothesis because, besides fluid-solid physicochemical conditions, there is a competition between the primary and secondary substrates to attract the supersaturated solution

and facilitate new nucleation events. The affinity for nucleation and growth of secondary minerals is higher adjacent or on top of the newly formed crystals than the original foreign substrate. The formation of the first nucleus on the substrate creates a secondary substrate with a higher potential (probability) to form the following nuclei. It incorporates another layer of complexity into the RTM, which is necessary to take into account to capture the reality of mineral growth in natural and engineered porous structures.

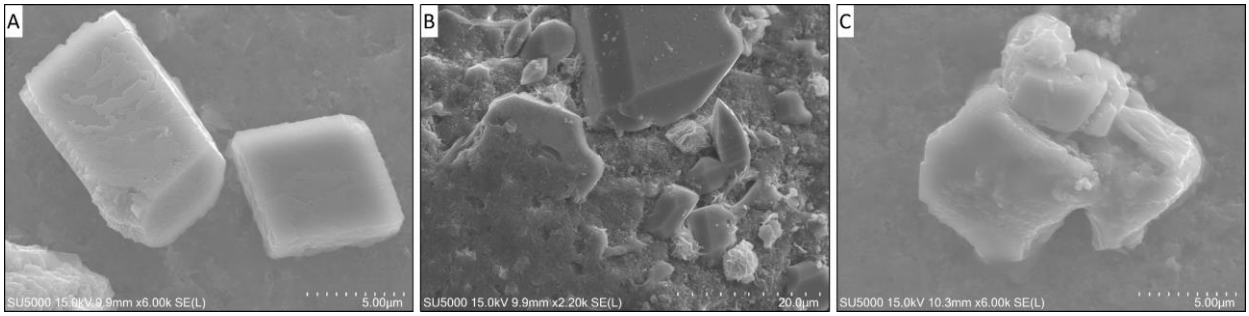

Figure 3: Mineral precipitation on the foreign substrate and previously precipitated crystals (secondary substrate). Crystallite formation with primitive non-crystalline forms on solid surfaces is shown, down to sub-micron resolution. Magnification and length scale of the SEM surface maps (secondary electron imaging) are given for each subfigure.

In other words, the marked difference between the interfacial free energy of the primary and secondary substrate determines the probability and affinity of new nucleation events. Furthermore, the preferential affinity to nucleate and grow on top and adjacent to secondary substrates also contributes to increased coalescence between the crystals (e.g., Figs. 1, 3-4). It, in turn, will attract increasingly more solutes towards the solid accumulation sites and, therefore, faster growth rate compared to areas with isolated and dispersed crystals. Such coalesced solid patches are of paramount importance as they significantly alter pore network geometry, and hence transport properties affecting fluid flow and solute transport pathways within the porous medium.

Figure 4 shows secondary electron imaging (SE SEM) of the substrate, where carbonate cement is present. As shown, in this favorable location, the available solute concentration for heterogeneous nucleation and precipitation is attracted and consumed by the previous carbonate patches (intergranular cement) owing to favorable interfacial free energy. As a result, the morphology of accumulated crystals is markedly different from what is shown previously. A semi-conform precipitation and growth pattern is illustrated in which individual crystals show a compact, coalesced, and overgrowth pattern. The co-presence of semi-conform precipitation patterns with coalesced crystalline geometries is also presented (Fig. 4c-d). Surface imaging of mineral precipitation in Figure 4 suggests that even on the carbonate cement and semi-conform accumulations, there is still a high enough probability to nucleate and grow crystalline geometries. Such a phenomenon will be of great importance when describing the effects of crystallization-driven clogging in reactive transport models. The three-dimensional structure and morphology of these crystals could modify or even block the pore structure and pathways affecting the subsequent flow and transport process. Without such information, our description of the effects of solute crystallization in porous materials would primarily rely on empirical parameters without adequate consideration of the actual physics governing the process.

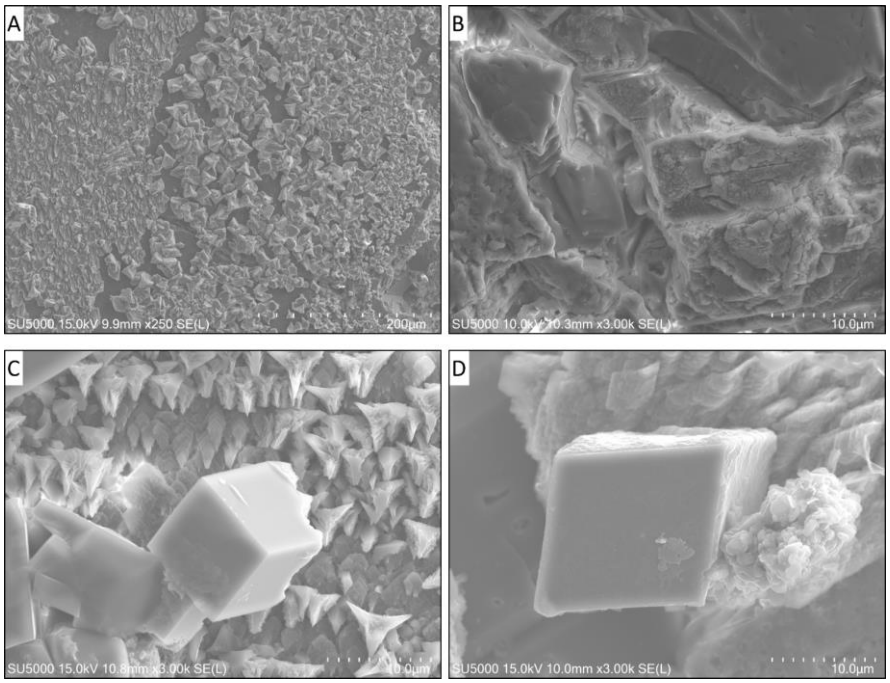

Figure 4: Secondary electron imaging (SE SEM) surface maps of calcium carbonate precipitation on the heterogeneous sandstone substrate, where intergranular carbonate cement is present. Semi-conform growth patterns and isolated crystalline mineral formation are illustrated. Magnification and length scale are given for each subfigure.

Detailed investigation of high-resolution EDS-SEM surface maps indicates that at lower supersaturation, more selective nucleation and growth phenomena occur where spots with more favorable surface characteristics will be selected first. At higher Ω, visual randomness and entropy are apparent. Even though a highly disordered system in Figure 1c-d is demonstrated where crystal growth is detectable almost everywhere, a detailed evaluation shows that several favored spots are still among the preferential locations. The favored sites for nucleation and subsequent growth are in the following order: (a) carbonate cement between the sandstone grains, owing to the considerably lower interfacial free energy between the precipitating phase and carbonate cement compared to other grain-forming minerals, (b) hollow and indentation surfaces such as holes and rough regions, (c) and around the grain edges, which can also be related to irregularity and roughness of the substrate among the grain edges providing preferential sites for crystallization compared to interior regions. A pronounced accumulation of coalesced crystals was observed around the grain edges, where hollow and indentation surfaces are present. Experimental observations indicate that spatial locations characterized with roughness and surface irregularities host more mineral nucleation and subsequent crystal growth. Given similar physicochemical conditions, these preferential sites are formed due to differences in surface characteristics manifested in surface free energy and increased surface-interface potential to attract solid formation and growth.

3.3 Substrate surface control on mineral precipitation

Our laboratory experiments showed several favorable locations for nucleation and growth. We conducted a series of LBM reactive transport simulations to study the effect of these preferential sites on certain parts of the substrate. Figure 5 shows the numerical results of modifying the interfacial free energy between the nucleating phase and the substrate. In Figure 5a, the secondary mineral precipitates are evenly distributed over the entire domain with similar growth patterns owing to the same σ (no favorable nucleation region exists as $\sigma_2/\sigma_1 = 1$). In Figure 5b, the bottom-left and top-right subdomains have smaller interfacial free energy than the rest of the domain ($\sigma_2/\sigma_1 = 0.5$). As a result, more mineral precipitation occurred in the areas with lower interfacial free energy. The lower the interfacial free energy (σ), the shorter the deterministic induction time (τ_N). The search for the probabilistic induction time (τ_P) takes place in the area expressed by a Gauss-Laplace probability density function with the τ_N as the average value ($\mu = \tau_N$). As a result, the probability of a nucleation event is higher in the areas with shorter induction times (here, due to lower interfacial free energy). Nucleation is necessary for growth, so a combination of more nucleation events and earlier nucleation events will result in more accumulation of mineral precipitation in favorable areas.

On the other hand, in Figure 5c, where the bottom-left and top-right portions have larger interfacial free energy than the rest of the domain ($\sigma_2/\sigma_1 = 1.6$), the mineral accumulations are concentrated in the inner part of the domain. Because of the probabilistic nature, nucleation events still occurred at high interfacial free energy regions. A comparison between simulation scenarios indicates how probabilistic mineral precipitation may control the evolution of porous geometries. The differences in interfacial free energy of subdomains (corner and inner regions) led to different nucleation locations, precipitation amounts, and growth patterns (Fig. 5).

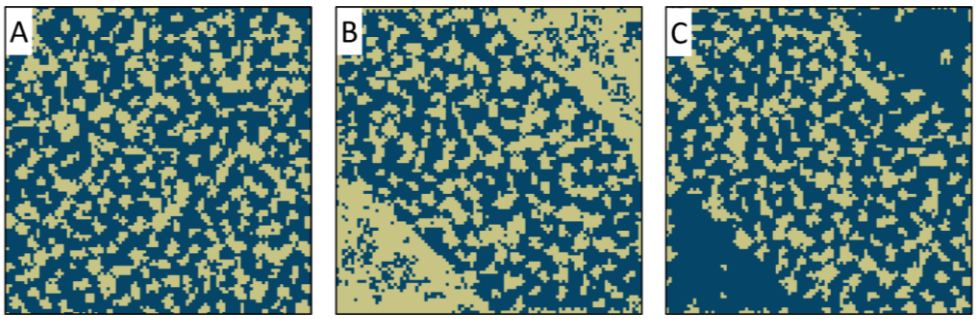

Figure 5: Numerical simulation of the impact of interfacial free energy between the nucleating phase and the substrate surface in a dual-medium solid. The proportionality ratio of subdomains is as follows σ_2/σ_1 = (a) 1, (b) 0.5, and (c) 1.6.

The experimental and numerical results highlight the impact of primary and secondary substrates and the importance of implementing favorable precipitation sites in the reactive transport modeling of porous media. Identifying, delineating, and predicting where nucleation and precipitation start under different boundary conditions is paramount. Without proper characterization of the spatial location of preferential crystallization and accumulation sites, the theoretical models aiming to describe flow and transport in natural and engineered porous geometries cannot realistically represent the physics and processes of fluid-rock interaction occurring in various geo-environmental and geoenergy applications (Nooraiepour et al., 2018; Masoudi et al., 2022, 2023).

ACKNOWLEDGMENTS

This publication has been produced with support from the "solid and salt precipitation kinetics during CO_2 injection into reservoir" project funded by Norway Grants (Norwegian Financial Mechanism 2014-2021, GRIEG Programme) under grant number UMO-2019/34/H/ST10/00564.

REFERENCES

Fazeli, H.; Nooraiepour, M.; Hellevang, H., 2020. Microfluidic Study of Fracture Dissolution in Carbonate-Rich Caprocks Subjected to CO_2-Charged Brine. Ind. Eng. Chem. Res. 59, doi:10.1021/acs.iecr.9b06048.

Hellevang, H.; Wolff-Boenisch, D.; Nooraiepour, M., 2019. Kinetic control on the distribution of secondary precipitates during CO_2-basalt interactions. In Proceedings of the E3S Web of Conferences; Vol. 98

Masoudi, M., Fazeli, H., Miri, R., Hellevang, H., 2021. Pore scale modeling and evaluation of clogging behavior of salt crystal aggregates in CO2-rich phase during carbon storage. Int. J. Greenh. Gas Control 111, 103475.

Masoudi, M.; Nooraiepour, M.; Hellevang, H., 2022. The Effect of Preferential Nucleation Sites on the Distribution of Secondary Mineral Precipitates. In Proceedings of the 83rd EAGE Annual Conference & Exhibition; European Association of Geoscientists & Engineers: Madrid, Spain.

Masoudi, M.; Nooraiepour, M.; Deng, H.; Hellevang, H., 2023. Mineral precipitation and geometry alteration in porous structures: How to upscale variations in permeability-porosity relationship? ACS Environmental Science and Technology.

Moghadam, J.N.; Nooraiepour, M.; Hellevang, H.; Mondol, N.H.; Aagaard, P., 2019. Relative permeability and residual gaseous CO2 saturation in the Jurassic Brentskardhaugen Bed sandstones, Wilhelmøya Subgroup, western central Spitsbergen, Svalbard. Nor. J. Geol., 99, 1–12.

Nooraiepour, Mohammad, Fazeli, H., Miri, R., Hellevang, H., 2018. Salt precipitation during injection of CO_2 into saline aquifers: Lab-on-chip experiments on glass and geomaterial microfluidic specimens. 14th Greenhouse Gas Control Technologies Conference (GHGT-14), October 2018, Melbourne, Australia.

Nooraiepour, M., Masoudi, M., Hellevang, H., 2021a. Probabilistic nucleation governs time, amount, and location of mineral precipitation and geometry evolution in the porous medium. Sci. Rep. 11, 16397.

Nooraiepour, M., Masoudi, M., Shokri, N., Hellevang, H., 2021b. Probabilistic nucleation and crystal growth in porous medium: New insights from calcium carbonate precipitation on primary and secondary substrates. ACS Omega, 6(42), 28072–28083.

Nooraiepour, M.; Masoudi, M.; Shorki, N.; Hellevang, H., 2022, Precipitation-Induced Geometry Evolution in Porous Media: Numerical and Experimental Insights Based on New Model on Probabilistic Nucleation and Mineral Growth. In SSRN Electronic Journal.